# Probing putative orbital differentiation effects via $Eu^{2+}$ spin dynamics in $Sr_{1-x}Eu_xFe_2As_2$

M. Radaelli,[1] M. M. Piva,[1,2] J. C. Souza,[1,*] G. G. Lesseux,[1] C. B. R. Jesus,[1,3] D. Tobia,[1,4] R. R. Urbano,[1] P. F. S. Rosa,[5] and P. G. Pagliuso[1,5]

[1]*Instituto de Física "Gleb Wataghin", UNICAMP, 13083-859 Campinas, São Paulo, Brazil*
[2]*Max Planck Institute for Chemical Physics of Solids, Nöthnitzer Strasse 40, D-01187 Dresden, Germany*
[3]*Departamento de Física, Universidade Federal de Sergipe, 49500-000 São Cristóvão, Sergipe, Brazil*
[4]*Instituto de Nanociencia y Nanotecnología (CNEA-CONICET), Centro Atómico Bariloche, Bariloche, Rio Negro, Argentina*
[5]*Los Alamos National Laboratory, Los Alamos, New Mexico 87545, USA*

(Received 6 October 2022; revised 1 February 2023; accepted 29 March 2023; published 12 April 2023)

In this work, we report x-ray powder diffraction, elemental analysis, electrical resistivity, magnetic susceptibility, specific heat, and electron spin resonance (ESR) in single crystals of $Sr_{1-x}Eu_xFe_2As_2$. We observed a breakdown of the previously reported scaling between the $Eu^{2+}$ Korringa relaxation rate obtained from ESR and the spin density wave temperature evolution for Sr-rich samples. This result suggests a distinct evolution of the orbital differentiation of the Fe 3*d* bands along the Sr-based series when compared to the Ba counterpart. We argue that this difference is related to a larger splitting between the structural (tetragonal-to-orthorhombic) and the Fe-driven spin density wave transitions induced by Eu doping in this series. In fact, our results indicate that the two transitions follow an opposite *x*-Eu dependence for Sr-concentrated samples. Our work shows that $Sr_{1-x}Eu_xFe_2As_2$ series and the comparison with their Ba-based counterparts are exciting platforms to be explored for understanding the interplay among orbital differentiation, magnetism, and structural distortions in the iron pnictides.

DOI: 10.1103/PhysRevB.107.134512

## I. INTRODUCTION

The interplay between magnetic order and superconductivity (SC) in several classes of unconventional superconductors suggests that magnetism can play an important role in the pairing mechanism for these systems [1]. Iron-based superconductors (FeSCs) are excellent materials for the study of this relation due to the possible presence of a spin-density-wave (SDW) antiferromagnetic order at high temperatures, which can be suppressed by chemical substitution and/or external applied pressure, inducing a superconducting state [2–4]. However, until now there is no complete microscopic understanding of the origin of the pairing mechanism in FeSCs [5].

Another element which may be important to the pairing mechanism in FeSCs is the nematic phase [6,7]. In particular, recent angle resolved photoemission spectroscopy results argue that the microscopic mechanism of the nematic phase should be the same between the iron $AFe_2As_2$ ($A$ = Ba, Sr, Ca) pnictides and Fe(Se,Te) chalcogenides [8–11]. Therefore, there are pressing open questions, such as the role of nematicity [12,13], orbital selectivity of the itinerant Fe 3*d* bands [14–22], and, particularly for the iron pnictides, carrier doping [23] to the appearance of a superconducting ground state.

Regarding doping, there are reports of SC induced by substitutions in all distinct crystallographic sites of the iron-based materials [3,4,24–26]. It is important to note that isoelectronic P substitution in the As site [3], along with the appearance of SC in stoichiometric iron pnictides under pressure [27], bring insights to the controversy about the actual role of charge doping in these materials [23]. Cosubstituted $BaFe_2As_2$ is regarded as one of the prime examples of charge doping [3,4]. However, x-ray absorption near edge structure measurements indicate no observable change in the Fe *K* edge spectra, and hence Co substitution does not add any electrons to the Fermi surface [28]. Furthermore, nuclear magnetic resonance measurements found the same quadrupolar frequency for the diluted regime of $Cu^{2+}$ and $Co^{2+}$ substituted $BaFe_2As_2$ samples, which again does not support the expectation that each Cu would deliver two extra 3*d* electrons into the Fermi surface compared to Co substitution [29,30].

Another crucial point is the role of orbital differentiation in the iron pnictides. This term is usually associated with the distinct weights of the Fe 3*d* orbitals ($d_{xy}$, $d_{xz}$, $d_{yz}$, $d_{x^2-y^2}$, and $d_{z^2}$) at the Fermi surface of these materials. This is a result of the actual structural symmetry of the Fe site and therefore is also strongly connected to tetragonal-to-orthorhombic transition at $T_s$ as well as to $T_{SDW}$. In particular, extended x-ray absorption fine structure measurements have shown that both applied pressure and chemical substitutions in $BaFe_2As_2$ are responsible for a shortening of the Fe-As bond length accompanied by a suppression of the SDW magnetic phase [31].

Previous electron spin resonance (ESR) reports show that this decrease in the Fe-As distance $d_{Fe\text{-}As}$ is closely connected to the suppression of the SDW magnetic phase transition

*Present address: Department of Condensed Matter Physics, Weizmann Institute of Science, Rehovot, Israel.

 

temperature $T_{SDW}$ and the localization of the Fe 3*d* electrons in the FeAs planes [32–34]. The increase of the planar character of the Fe 3*d* orbitals, favoring the occupation of the *xy* and $x^2$-$y^2$ orbitals at the Fermi surface, may be a key ingredient in the physics of FeSCs [14]. Finally, recent scanning tunneling spectroscopy measurements in $Ba_{0.6}K_{0.4}Fe_2As_2$ give interesting insights about the orbital selectivity, as it was found that tunneling on each termination surface of this compound probes superconductivity through selecting distinct Fe 3d orbitals [22]. All the above results hint that SC, orbital differentiation of the itinerant Fe 3*d* bands, and the Fe-As bond length are intimately connected for pnictides.

In order to further understand and generalize the role of the orbital differentiation to the physics of the FeAs-based materials, it is instructive to tune the coupling between structural and magnetic orders in distinct members of this family. While for $BaFe_2As_2$ the tetragonal-to-orthorhombic transition at $T_s$ is either a weak first-order or a second-order transition [35], for the counterpart compound $SrFe_2As_2$ the structural transition is first order [36–39]. As a consequence, the structural and magnetic orders are presumably strongly coupled, which weakens the nematic phase [39].

In this work, we have performed ESR measurements in $Sr_{1-x}Eu_xFe_2As_2$ single crystals. ESR is a microscopic probe which can detect changes in the Fe 3*d* bands at the Fermi level through an analysis of the $Eu^{2+}$ spin dynamics [32,33]. More specifically, the exchange interaction *J* between the conduction electrons (*ce*) and the $Eu^{2+}$ local moments depends on the overlap between the atomic orbitals [32,33]. For $Sr_{1-x}Eu_xFe_2As_2$, the $Eu^{2+}$ local moments are our ESR paramagnetic probes located out of the FeAs plane. Therefore, an increase of the planar *xy* orbital contribution would decrease the exchange interaction between *ce* and the $Eu^{2+}$ moments. Conversely, an increase in the *yz* or *xz* orbital contributions would increase orbital overlap with the ESR probe. Such exchange interaction will be reflected in the relaxation of our probe, through the spin-flip scattering between the $Eu^{2+}$ local moments and the carriers (Korringa mechanism) [40–42], and in the *g* value, extracted from the $Eu^{2+}$ resonance field [40–42]. Our data unveil that the Korringa relaxation rate *b*, and consequently the exchange *J*, does not follow $T_{SDW}$ in Sr-rich samples. This result indicates that the orbital differentiation of the Fe 3*d* orbitals is instead connected with $T_s$. We argue that $T_s$ and $T_{SDW}$ follow an opposite dependence as a function of $Eu^{2+}$ substitution in Sr-rich samples. Our work shows that the $Sr_{1-x}Eu_xFe_2As_2$ system may be an interesting playground to understand the role of different interactions in the physics of FeSCs.

## II. METHODS

Single crystalline samples of $Sr_{1-x}Eu_xFe_2As_2$ were grown by the In-flux method [43,44]. The $I4/mmm$ crystalline structure was confirmed by x-ray powder diffraction at room temperature using a commercial diffractometer. The synthesized phase and the actual $Eu^{2+}$ content in the samples were determined by elemental analysis using energy dispersive x-ray spectroscopy (EDS). High-temperature X-band ($\nu = 9.34$ GHz) ESR measurements were performed in a commercial spectrometer using appropriated resonators and temperature-controller systems. Both single crystals and powdered samples were used in the ESR experiments to study anisotropic effects and to increase the ESR signal-to-noise ratio, respectively. Nuclear magnetic resonance (NMR) experiments in single crystals of undoped $SrFe_2As_2$ were carried out using a NMR probe equipped with a goniometer for fine *in situ* alignment of the crystallographic axes with the external applied magnetic field. The field-swept $^{75}$As NMR spectra ($I = 3/2$; $\gamma/2\pi = 7.2919$ MHz/T) were obtained by stepwise summing the Fourier transform of the spin-echo signals. Magnetic susceptibility measurements were performed in Superconducting Quantum Interference Device (SQUID)-based commercial magnetometer. Specific heat measurements were done in a small-mass calorimeter system that employs a quasi-adiabatic thermal relaxation technique. In-plane electrical resistivity was obtained in a commercial low-frequency equipment using the standard four-probe technique and with the current applied in the *ab* plane.

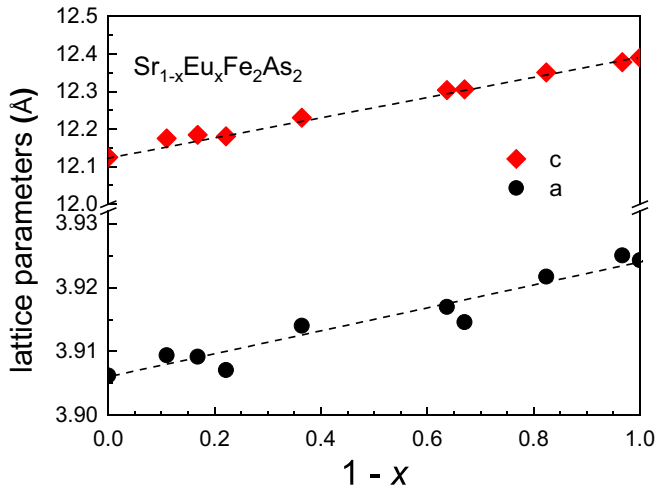


FIG. 1. Lattice parameters *a* and *c* for $Sr_{1-x}Eu_xFe_2As_2$. The dashed lines are guides to the eye.

## III. RESULTS AND DISCUSSION

Figure 1 displays the lattice parameters obtained from Rietveld refinements of the $Sr_{1-x}Eu_xFe_2As_2$ x-ray powder diffraction. Both *a* and *c* decrease linearly with increasing $Eu^{2+}$ content, indicating a homogeneous substitution of $Sr^{2+}$ by $Eu^{2+}$, in agreement with Vegard's law [45]. However, *c* is more affected (1.6% total variation) than *a* (0.4% total variation) with increasing $Eu^{2+}$ substitution. The lattice parameters present similar values as in previous reports [2]. No changes on Fe-As local geometry were detected in these measurements along this series within the experimental uncertainty.

Figure 2 presents the specific heat ($c_p$), magnetic susceptibility ($\chi$), and resistivity ($\rho$) as a function of temperature for $Sr_{1-x}Eu_xFe_2As_2$. One can clearly see a sharp peak at high temperatures in Fig. 2(a), which can be associated with both the structural and SDW phase transition. One can see that this anomaly initially increases and becomes sharper for the $1 - x = 0.97$ sample and then decreases as a function of $Eu^{2+}$ concentration. This decrease is consistent with the expected behavior of the $T_{SDW}$ since $EuFe_2As_2$ shows a lower $T_{SDW}$ ($\approx$192 K) when compared to $SrFe_2As_2$ ($\approx$205 K). A small

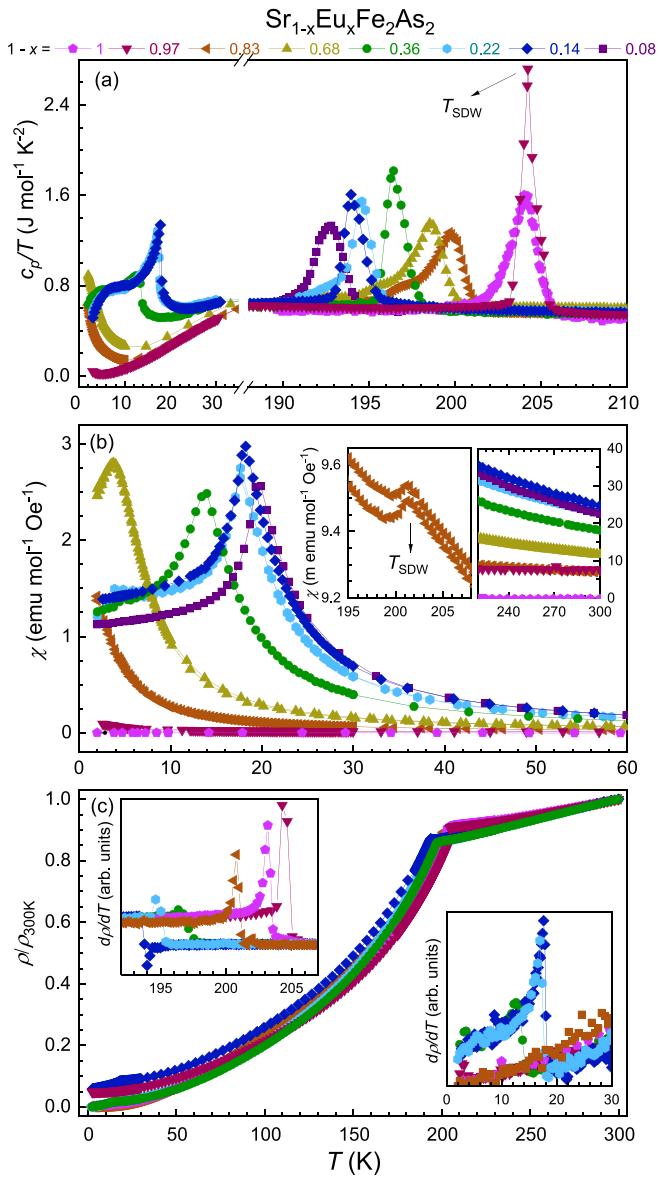


FIG. 2. Temperature dependence of (a) specific heat, (b) magnetic susceptibility, and (c) dc resistivity for $Sr_{1-x}Eu_xFe_2As_2$. $\chi$ measurements were done with applied field $H = 300$ Oe parallel to the *ab* plane. The top insets in panel (b) show the signature of $T_{SDW}$ and the data at high temperatures. The insets in panel (c) show the derivative of the resistivity near $T_{SDW}$ (left) and $T_N$ (right).

shoulder is visible at intermediate concentrations, which could be related with disorder effects producing a distribution of $T_{SDW}$s in the crystals. In contrast to substituted $BaFe_2As_2$ samples, no splitting of $T_S$ and $T_{SDW}$ is observed in specific heat measurements for $Sr_{1-x}Eu_xFe_2As_2$. At low temperatures, a rise in $c_p/T$ is observed for $Sr^{2+}$-rich samples. Such rise is caused by $Eu^{2+}$-$Eu^{2+}$ interactions, similar to $Ba_{1-x}Eu_xFe_2As_2$ [32]. For higher $Eu^{2+}$ concentrations ($1 - x \leqslant 0.36$), antiferromagnetic order of the $Eu^{2+}$ local moments occurs, which generates a low-temperature peak in $c_p/T$.

The magnetic susceptibility as a function of temperature is displayed in Fig. 2(b). The magnetic field $H = 300$ Oe was applied parallel to the *ab* plane. The data for $Eu^{2+}$-substituted samples, corrected for the core diamagnetism, were fitted to a Curie-Weiss law at high temperatures (220 K $\leqslant T \leqslant$ 300 K) (see the top right inset of Fig. 2). From these fits we estimate the $Eu^{2+}$ concentration, assuming each ion carries an effective magnetic moment of 7.94 $\mu_B$. All $Eu^{2+}$ concentrations are in agreement with the concentration obtained from EDS measurements. We also extracted the Pauli contribution $\chi_0 =$ 0.002(3) emu/mol-Oe for all concentrations. Regarding the magnetic transitions, $T_{SDW}$ can be seen as a kink in $\chi$ for all concentrations, as shown in one example in the top left inset of Fig. 2(b). At low temperatures, one can see a clear monotonic decrease of $T_N$ as a function of $Eu^{2+}$ concentration, which is consistent with specific heat measurements.

The temperature dependence of normalized resistivity ($\rho/\rho_{300K}$ is illustrated in Fig. 2(c). At high temperatures, a metallic behavior is observed for all $x$. A clear kink characterizes $T_{SDW}$ for all samples. The derivative of $\rho$ only shows one peak at high temperatures (left inset), in agreement with the heat capacity data. The estimated transition width from these data for the pure $SrFe_2As_2$ samples is ≈2 K, which indicates that if there is a separation between $T_s$ and $T_{SDW}$ in these sample, it should be smaller than 2 K. The right inset of Fig. 2(c) shows the derivative of the resistivity at low temperatures, in which we obtained a peak that can be associated with $T_N$. In fact, the transition temperatures extracted from resistivity, specific heat, and magnetic susceptibility are consistent with each other.

To gain microscopic insights regarding the possible splitting of $T_S$ and $T_{SDW}$ in $Sr_{1-x}Eu_xFe_2As_2$ we have performed NMR experiments in single crystals of undoped $SrFe_2As_2$. Figure 3 shows the $^{75}$As NMR signal for an In-grown $SrFe_2As_2$ single crystal within the 204 to 200 K temperature range with $H \perp c$. At 204 K, the narrow line at $H \approx 9.35$ T corresponds to the $(-1/2 \leftrightarrow 1/2)$ transition in the tetragonal/paramagnetic phase of $SrFe_2As_2$ near the structural/SDW transitions. The intensity of the resonance dramatically disappears within a 2 K range as the sample is cooled through the structural/SDW transitions. In addition, no broad line associated with the orthorhombic phase or ordered magnetic domains with strong magnetic interactions emerges in this range, as previously observed for doped $BaFe_2As_2$ [46]. This result reveals that the presence of even stronger magnetic interactions below $T_{SDW}$ in $SrFe_2As_2$ are affecting the NMR line associated to the orthorhombic/ordered phase. As a result, the resonance line is wiped out due to quite fast relaxation below $T_s$ [46].

The presence of even stronger magnetic interactions in the ordered state $SrFe_2As_2$ when compared to $BaFe_2As_2$ indicates that most of the available entropy of the structural/SDW transitions rely on the magnetic transition. This would make it harder to track the $T_S$ evolution in the $Sr_{1-x}Eu_xFe_2As_2$ series using macroscopic measurements.

Now, to obtain microscopic insights about the orbital differentiation through the $Eu^{2+}$ spin dynamics evolution along the series, we have performed ESR in $Sr_{1-x}Eu_xFe_2As_2$ crystals. Figure 4 shows the summary of our $Eu^{2+}$ $X$-band ESR. The left panel of Fig. 4 shows the $Eu^{2+}$ ESR spectra at $T =$ 200 K for $1 - x = 0.83$, 0.68, 0.22, and 0.14. The magenta solid lines are the best fits to the $Eu^{2+}$ ESR spectra considering an admixture of absorption and dispersion derivatives. The

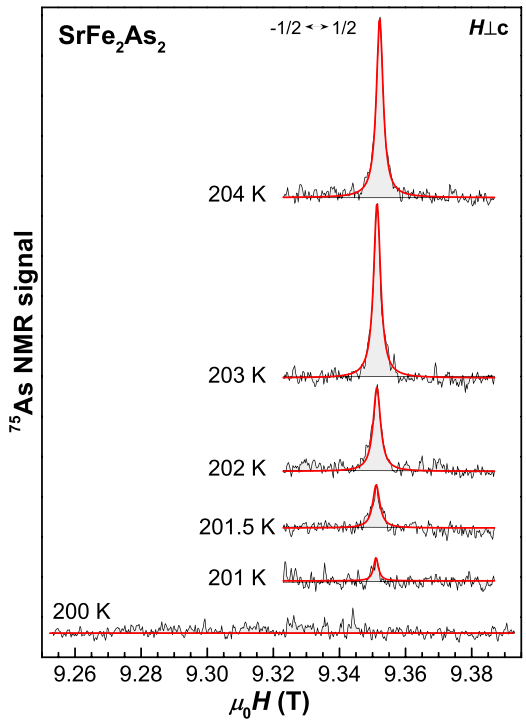


FIG. 3. $^{75}$As NMR central transition ($-1/2 \leftrightarrow 1/2$) at $\nu = 68.5878$ MHz for the In-grown $SrFe_2As_2$ single crystal, within the 204 to 200 K temperature range with $H \perp c$. The red solid lines are Lorentzian fits to the spectra.

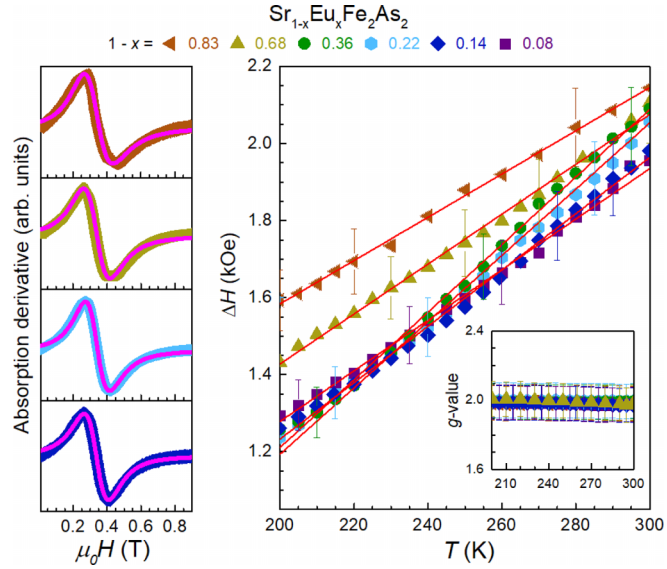


FIG. 4. Left panel: $X$-band $Eu^{2+}$ ESR spectra at $T = 200K$ of $Sr_{1-x}Eu_xFe_2As_2$ for $1-x = 0.83, 0.68, 0.22$, and $0.14$ (no ESR signal was observed for $1-x = 0.97$). The magenta solid lines are fits described into the text. Right panel: Temperature dependence of the linewidth $\Delta H$. The red solid lines are the best linear fits obtained. The right inset shows the temperature dependence of the $g$ value.

power absorption derivative ($dP/dH$) as a function of the applied field $H$ can be expressed as

$$\frac{dP}{dH} \propto (1-\lambda)\frac{d}{dx}\left(\frac{1}{1+x^2}\right) + \lambda\frac{d}{dx}\left(\frac{x}{1+x^2}\right), \qquad (1)$$

where the first term is the absorption component, the second term is the dispersion component, $\lambda$ is the asymmetric parameter of the (Dysonian) line shape, and $x = 2(H - H_r)/\Delta H$, wherein $H_r$ is the $Eu^{2+}$ resonance field and $\Delta H$ the $Eu^{2+}$ ESR linewidth. The Dysonian line shape was used to fit the ESR spectra of Fig. 4 and extract the $Eu^{2+}$ ESR $g$ values and linewidth [41,42,47,48].

The right panel of Fig. 4 shows the temperature evolution of $Eu^{2+}$ $\Delta H$ for 200 K $\leqslant T \leqslant$ 300 K for different $Eu^{2+}$ concentrations. Toward high temperatures, there is a clear linear increase of $\Delta H$, which suggests a Korringa relaxation mechanism [41,42]. This linear $\Delta H$ increase as a function of temperature is observed for all samples. Performing a linear fit of $\Delta H(T)$, $\Delta H = \Delta H_0 + bT$, where $\Delta H_0$ is the $Eu^{2+}$ residual linewidth, we obtain the Korringa rate $b$ for all concentrations. For $EuFe_2As_2$, we obtained $b = 6.6$ Oe/K, which is in good agreement with previous reports [32,49,50]. The $g$ factor of the $Eu^{2+}$ ESR spectra is $g \approx 2$ for all temperatures and concentrations (right inset of Fig. 4).

Figure 5 displays the phase diagram for $Sr_{1-x}Eu_xFe_2As_2$ as a function of $1-x$. Both $T_{SDW}$ and $T_N$ were obtained using the macroscopic measurements detailed above. For comparison, we also present the evolution of the Korringa relaxation rate $b$ as a function of the concentration $1-x$. We note that $T_{SDW}$ increases and $T_N$ decreases with the decrease of $Eu^{2+}$ concentration. For $1-x \geqslant 0.75$, the $Eu^{2+}$ AFM transition is no longer identified above $T = 2$ K. Interestingly the $Eu^{2+}$ AFM ordering in $Sr_{1-x}Eu_xFe_2As_2$ has higher $T_N$ than in $Ba_{1-x}Eu_xFe_2As_2$, indicating a larger $Eu^{2+}$-$Eu^{2+}$ magnetic interaction [36–39].

It is worth noting the difference in the trend of the $b$ rate as a function of $1-x$ in comparison with $Ba_{1-x}Eu_xFe_2As_2$ [32,49,50]. In the Ba series, the $b$ rate follows the same trend of $T_{SDW}$ as function of Eu concentration, whereas in $Sr_{1-x}Eu_xFe_2As_2$, the $b$ rate has the same trend of $T_{SDW}$ only at higher concentrations of $Eu^{2+}$ ($1-x \leqslant 0.5$).

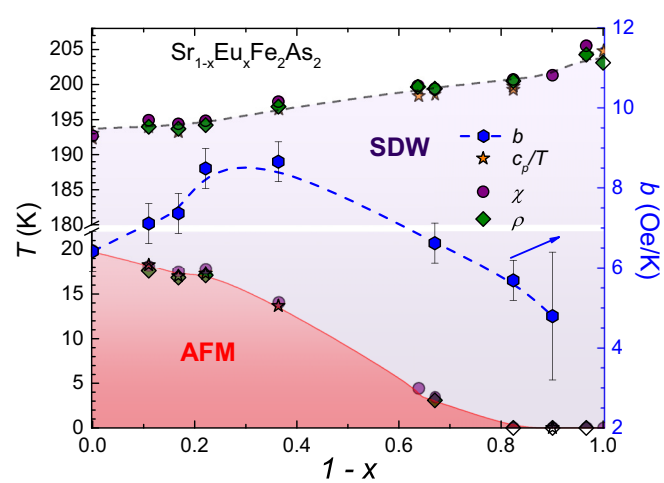


FIG. 5. $Sr_{1-x}Eu_xFe_2As_2$ phase diagram and the comparison with the Korringa rate as a function of $Eu^{2+}$ concentration. The solid and dashed lines are guides to the eyes.

This difference in the Korringa rate $b$ scaling between Sr and Ba compounds can be understood by analyzing the exchange interaction $J$ between the $Eu^{2+}$ local moments and the *ce* in these compounds. Assuming that bottleneck, dynamic, electron-electron correlation, $\mathbf{q}$ dependence, and multiple bands effects are not present in the interaction between the $Eu^{2+}$ local moments and the Fe 3*d* *ce* [34], the $b$ rate and the ESR $g$ shift can be written as [41,42]

$$b = \frac{\pi k_B}{g\mu_B} J_{fd}^2 \eta^2(E_F), \tag{2}$$

$$\Delta g \equiv g - g_{\text{insulator}} = J_{fd}\eta(E_F), \tag{3}$$

where $J_{fd}$ is the effective exchange interaction between the $Eu^{2+}$ local moment and the *ce* in the absence of *ce* momentum transfer, $\eta(E_F)$ is the density of states for one spin direction at the Fermi surface, $\kappa_B$ is the Boltzmann constant, $\mu_B$ is the Bohr magneton, and $g_{\text{insulator}} = 1.993$ is the $Eu^{2+}$ $g$ value in an insulator. When Eqs. (1) and (2) are applicable, we have the following identity:

$$b = \frac{\pi k_B}{g\mu_B} \Delta g^2. \tag{4}$$

Figure 5 shows that the $b$ rate has a dependence with $Eu^{2+}$ concentration, while the $g$ value is concentration independent. This is a clear indication that Eq. (4) is no longer valid and we should take into consideration the $\mathbf{q}$ dependence of the exchange interaction, $J_{fd}(\mathbf{q})$ [32,33,42]. At the $Eu^{2+}$ site, the $g$ shift probes the *ce* polarization ($\mathbf{q} = 0$) and the Korringa rate probes the average over the Fermi surface of the *ce* momentum transfer ($0 \leqslant q \leqslant 2k_F$) [41,42]. In other words, The $Eu^{2+}$ ESR linewidth Korringa rate, $b$, depends on the average of the $q$-dependent effective exchange interaction between the $Eu^{2+}$ local moment and the Fe 3*d* conduction electrons averaged over the whole Fermi surface, $J_{fd}(\mathbf{q})$, which is strongly connected to the Fe 3*d* orbital differentiation and the weight of the Fe 3*d* orbitals ($d_{xy}$, $d_{xz}$, $d_{yz}$, $d_{x^2-y^2}$, and $d_{z^2}$) at the Fermi surface.

Bottleneck effects are not present because, in the diluted regime, the Korringa rate increases with increasing $Eu^{2+}$ concentration [41]. If dynamic effects were present, the $g$ value should be $T$ dependent, which is not the case [51]. Finally, multiple bands effects can be neglected due to the contribution at the Fermi surface being only from Fe 3*d* electrons. The remaining point is the contribution of electron-electron interactions. The estimated Pauli magnetic susceptibility, assuming a free *ce* gas model, for $SrFe_2As_2$ ($\chi_{\text{theoretical}} \approx$ 62 μemu/mol-Oe) is two orders of magnitude smaller compared to the experimental value $\chi_0 = 2(3)$ memu/mol-Oe, which means that electron-electron correlations are important to our ESR analysis. This is consistent with recent inelastic neutron scattering results in $BaFe_2As_2$, which also show the importance of electron-electron correlations in iron pnictides [52,53]. With the $\mathbf{q}$ dependence and electron-electron interaction assumptions, Eqs. (1) and (2) should be rewritten as

$$b = \frac{\pi k_B}{g\mu_B} \langle J_{fd}^2(\mathbf{q})\rangle \eta^2(E_F) \frac{K(\alpha)}{(1-\alpha)^2}, \tag{5}$$

$$\Delta g = J_{fd}(\mathbf{0}) \frac{\eta(E_F)}{(1-\alpha)}, \tag{6}$$

where $(1-\alpha)^{-1}$ is the Stoner enhancement factor [54,55] and $K(\alpha)$ is the Korringa exchange enhancement factor [56,57].

Importantly, the $Eu^{2+}$ ESR $g$ value is $x$ independent (inset of Fig. 4). Therefore, we can infer that the density of states for one spin direction at the Fermi surface $\eta(E_F)$ and the Stoner enhancement factor $\alpha$ are nearly $x$ independent within the experimental error bars [see Eq. (6)]. Consequently, the $q$-dependent effective exchange interaction averaged over the whole Fermi surface, $\langle J_{fd}^2(\mathbf{q})\rangle$ is more affected by doping than its value for $\boldsymbol{q} = 0$, which clearly indicates an evolution of the topology of the Fermi surface with $x$, since $J_{fd}(\mathbf{q})$ is just the Fourier transform of $J_{fd}(\mathbf{r})$.

Previous studies in $Ba_{1-x}Eu_xFe_2As_2$ series have shown a decrease in $\langle J_{fd}^2(\mathbf{q})\rangle$ as $T_{SDW}$ is suppressed, indicating that the *ce* bands which overlap with $Eu^{2+}$ 4*f* states are becoming more anisotropic, i.e., the $d_{xy}$ orbitals are increasing their role at the Fermi surface. In real space, this is reflected by the increasing of the separation between the $Eu^{2+}$ site and the *ce*, which characterizes a localization of Fe 3*d* conduction electrons in the FeAs plane. As $Ba^{2+}$ and $Eu^{2+}$ are isoelectronic, there is no introduction of carriers, and therefore the evolution in the electronic structures is likely due to subtle changes in the tetragonal crystal structures (and consequently in the Fe-As bonds). Hence, the orbital differentiation and the occupation of the Fe 3*d* orbitals should follow the structural distortion $T_s$, which is coupled to $T_{SDW}$ in $BaFe_2As_2$ [32,33].

In the low $Eu^{2+}$-concentration regime for $Sr_{1-x}Eu_xFe_2As_2$, we have obtained a different scaling between $b$ and $T_{SDW}$—while the first increases, the second decreases, apart from the possible small initial increase of the both $T_s$ and $T_{SDW}$ for the $1-x = 0.97$ sample. This is a hint that $T_s$ and $T_{SDW}$ are not tracking each other for Sr-rich samples, most likely because of the coexisting magnetically ordered orthorhombic and paramagnetic tetragonal domains are more likely to persist over an larger temperature range above $T_{SDW}$ in the Eu-substituted $SrFe_2As_2$ compared with their $BaFe_2As_2$ counterparts [32,33,36–39]. This effect was clearly observed in Raman scattering, synchrotron x-ray diffraction, specific heat, resistivity, and magnetic susceptibility measurements performed in $Sr(Fe_{1-x}Co_x)_2As_2$ [$x = 0.20(3)$] single crystals [58].

Microscopically, the increase of $b$ reveals an enhancement of $\langle J_{fd}^2(\mathbf{q})\rangle$ as $T_{SDW}$ is suppressed, indicating a larger contribution of the $d_{xz/yz}$ orbital character. This increase in the axial ($d_{xz/yz}$) orbital contribution is related to an increase in $T_s$ as the SDW phase is suppressed, suggesting a possible initial splitting between $T_s$ and $T_{SDW}$ as they follow opposite directions as a function Eu concentration in the Sr-rich regime. Presumably, apart from the initial increase of both $T_s$ and $T_{SDW}$ where the anomalies in our data become sharper, $T_{SDW}$ starts to decrease with the larger amount of entropy associated with it, which makes $T_s$ practically undetectable in our macroscopic measurements. However, the Eu-$x$ dependence of $T_s$ can still be tracked by our ESR measurements.

Therefore, in contrast with previous reports [32,33], we argue that the separation between $T_s$ and $T_{SDW}$ is within a 2 K range for pure $SrFe_2As_2$, but they are following an opposite evolution as a function of Eu doping in the low $Eu^{2+}$-concentration regime. This occurs most likely due to

the strong magnetic fluctuations present in this compound [32,33,36–39,58], which allows the coexistence of orthorhombic and tetragonal domains over a larger temperature range above $T_{SDW}$ and below $T_s$. In the high $Eu^{2+}$-concentration region, $1 - x \leqslant 0.5$, the suppression of the SDW phase follows the suppression of the $Eu^{2+}$ ESR Korringa rate, consistent with a localization of the 3*d* electrons in the FeAs plane, similar to the $BaFe_2As_2$ series which indicates that $T_s$ is accompanying the same trend of $T_{SDW}$. However, it is worth emphasizing that modeling the microscopic interaction between Fe 3d electrons and the $Eu^{2+}$ ESR probes is a open challenge and further experiments such as nuclear magnetic resonance, x-ray absorption fine structure, and high-resolution x-ray diffraction as a function of temperature in the Eu-doped $(Ba,Sr)Fe_2As_2$ could be useful to understand this main difference between the $BaFe_2As_2$ and $SrFe_2As_2$ compounds.

## IV. CONCLUSIONS

In summary, we present a detailed experimental characterization of In-flux grown $Sr_{1-x}Eu_xFe_2As_2$ single crystals by x-ray powder diffraction, elemental analysis, specific heat, magnetic susceptibility, electrical resistivity, and electron spin resonance (ESR). Our ESR results may indicate a different evolution of the orbital differentiation of the Fe 3*d* bands as the spin density wave is suppressed compared to the Ba series. We suggest that this anomalous evolution is related to an Eu-induced higher splitting between the structural phase transition and the spin-density-wave transition in the dilute regime for $Sr_{1-x}Eu_xFe_2As_2$. These results suggest that the orbital differentiation of the 3*d* bands of Fe in these materials seems to be governed by subtle structural distortions.

## ACKNOWLEDGMENTS

This work was supported by FAPESP (Grants No. 2015/09701-7, No. 2017/10581-1, No. 2012/04870-7, No. 2018/11364-7, and No. 2020/12283-0), CNPq (Grants No. 311783/2021-0, No. 309483/2018-2, No. 314587/2021-7, No. 442230/2014-1, and No. 304649/2013-9), CAPES, and FINEP-Brazil. The authors would like to acknowledge the Brazilian Nanotechnology National Laboratory (LNNano Project Inspect No. 14958) for providing the equipment and technical support for the experiments involving scanning electron microscopy. Work at Los Alamos was supported by the U.S. Department of Energy, Office of Basic Energy Sciences, Division of Materials Science and Engineering: Project Quantum Fluctuations in Narrow-Band Systems.

[1] P. Monthoux, D. Pines, and G. G. Lonzarich, Superconductivity without phonons, Nature (London) **450**, 1177 (2007).

[2] J. W. Lynn, and P. Dai, Neutron studies of the iron-based family of high $T_c$ magnetic superconductors, Phys. C (Amsterdam, Neth.) **469**, 469 (2009).

[3] J. Paglione, and R. L. Greene, High-temperature superconductivity in iron-based materials, Nat. Phys. **6**, 645 (2010).

[4] G. R. Stewart, Superconductivity in iron compounds, Rev. Mod. Phys. **83**, 1589 (2011).

[5] G. Biswal and K. L. Mohanta, A recent review on iron-based superconductor, Materials Today: Proceedings **35**, 207 (2021).

[6] R. M. Fernandes, A. V. Chubukov, and J. Schmalian, What drives nematic order in iron-based superconductors? Nat. Phys. **10**, 97 (2014).

[7] M. H. Christensen, J. Kang, B. M. Andersen and R. M. Fernandes, Spin-driven nematic instability of the multiorbital Hubbard model: Application to iron-based superconductors, Phys. Rev. B **93**, 085136 (2016).

[8] H. Pfau, C. R. Rotundu, J. C. Palmstrom, S. D. Chen, M. Hashimoto, D. Lu, A. F. Kemper, I. R. Fisher, and Z.-X. Shen, Detailed band structure of twinned and detwinned $BaFe_2As_2$ studied with angle-resolved photoemission spectroscopy, Phys. Rev. B **99**, 035118 (2019).

[9] H. Pfau, S. D. Chen, M. Yi, M. Hashimoto, C. R. Rotundu, J. C. Palmstrom, T. Chen, P. Dai, J. Straquadine, A. Hristov *et al.*, Momentum Dependence of the Nematic Order Parameter in Iron-Based Superconductors, Phys. Rev. Lett. **123**, 066402 (2019).

[10] M. Yi, H. Pfau, Y. Zhang, Y. He, H. Wu, T. Chen, Z. R. Ye, M. Hashimoto, R. Yu, Q. Si *et al.*, Nematic Energy Scale and the Missing Electron Pocket in FeSe, Phys. Rev. X **9**, 041049 (2019).

[11] M. Yi, Y. Zhang, Z.-X. Shen, and D. Lu, Role of the orbital degree of freedom in iron-based superconductors, npj Quantum Mater. **2**, 57 (2017).

[12] J. Kang, R. M. Fernandes, and A. Chubukov, Superconductivity in FeSe: The Role of Nematic Order, Phys. Rev. Lett. **120**, 267001 (2018).

[13] S.-H. Baek, J. M. Ok, J. S. Kim, S. Aswartham, I. Morozov, D. Chareev, T. Urata, K. Tanigaki, Y. Tanabe, B. Büchner *et al.*, Separate tuning of nematicity and spin fluctuations to unravel the origin of superconductivity in FeSe, npj Quantum Mater. **5**, 8 (2020).

[14] Z. P. Yin, K. Haule, and G. Kotliar, Kinetic frustration and the nature of the magnetic and paramagnetic states in iron pnictides and iron chalcogenides, Nat. Mater. **10**, 932 (2011).

[15] F. Wang and D.-H. Lee, The electron-pairing mechanism of iron-based superconductors, Science **332**, 200 (2011).

[16] P. O. Sprau, A. Kostin, A. Kreisel, A. E. Böhmer, V. Taufour, P. C. Canfield, S. Mukherjee, P. J. Hirschfeld, B. M. Andersen, and J. C. Séamus Davis, Discovery of orbital-selective Cooper pairing in FeSe, Science **357**, 75 (2017).

[17] E. M. Nica, R. Yu, and Q. Si, Orbital-selective pairing and superconductivity in iron selenides, npj Quantum Mater. **2**, 24 (2017).

[18] A. Kreisel, B. M. Andersen, P. O. Sprau, A. Kostin, J. C. Séamus Davis, and P. J. Hirschfeld, Orbital selective pairing and gap structures of iron-based superconductors, Phys. Rev. B **95**, 174504 (2017).

[19] A. Kostin, P. O. Sprau, A. Kreisel, Y. X. Chong, A. E. Böhmer, P. C. Canfield, P. J. Hirschfeld, B. M. Andersen, and J. C.

Séamus Davis, Imaging orbital-selective quasiparticles in the Hund's metal state of FeSe, Nat. Mater. **17**, 869 (2018).

[20] H. Hu, R. Yu, E. M. Nica, J.-X. Zhu, and Q. Si, Orbital-selective superconductivity in the nematic phase of FeSe, Phys. Rev. B **98**, 220503(R) (2018).

[21] R. Yu, H. Hu, E. M. Nica, J.-X. Zhu, and Q. Si, Orbital selectivity in electron correlations and superconducting pairing of iron-based superconductors, Front. Phys. Sec. Condensed Matter Physics **9**, 578347 (2021).

[22] J.-X. Yin, X.-X. Wu, J. Li, Z. Wu, J.-H. Wang, C.-S. Ting, P.-H. Hor, X. J. Liang, C. L. Zhang, P. Dai *et al.*, Orbital selectivity of layer-resolved tunneling in the iron-based superconductor $Ba_{0.6}K_{0.4}Fe_2As_2$, Phys. Rev. B **102**, 054515 (2020).

[23] S. Ideta, T. Yoshida, T. Nishi, A. Fujimori, Y. Kotani, K. Ono, Y. Nakashima, S. Yamaichi, T. Sasagawa, M. Nakajima *et al.*, Dependence of Carrier Doping on the Impurity Potential in Transition-Metal-Substituted FeAs-Based Superconductors, Phys. Rev. Lett. **110**, 107007 (2013).

[24] S. Wu, Y. Song, Y. He, A. Frano, M. Yi, X. Chen, H. Uchiyama, A. Alatas, A. H. Said, L. Wang *et al.*, Short-Range Nematic Fluctuations in $Sr_{1-x}Na_xFe_2As_2$, Phys. Rev. Lett. **126**, 107001 (2021).

[25] S. R. Saha, N. P. Butch, K. Kirshenbaum, and J. Paglione, Evolution of bulk superconductivity in $SrFe_2As_2$ with Ni substitution, Phys. Rev. B **79**, 224519 (2009).

[26] S. Nandi, W. T. Jin, Y. Xiao, Y. Su, S. Price, D. K. Shukla, J. Strempfer, H. S. Jeevan, P. Gegenwart, and T. Brückel, Coexistence of superconductivity and ferromagnetism in P-doped $EuFe_2As_2$, Phys. Rev. B **89**, 014512 (2014).

[27] P. L. Alireza, Y. T. C. Ko, J. Gillett, C. M. Petrone, J. M. Cole, G. G. Lonzarich, and S. E. Sebastian, Superconductivity up to 29 K in $SrFe_2As_2$ and $BaFe_2As_2$ at high pressures, J. Phys.: Condens. Matter **21**, 012208 (2009).

[28] E. M. Bittar, C. Adriano, T. M. Garitezi, P. F. S. Rosa, L. Mendonça-Ferreira, F. Garcia, G. de M. Azevedo, P. G. Pagliuso, and E. Granado, Co-Substitution Effects on the Fe Valence in the $BaFe_2As_2$ Superconducting Compound: A Study of Hard X-Ray Absorption Spectroscopy, Phys. Rev. Lett. **107**, 267402 (2011).

[29] T. M. Garitezi, G. G. Lesseux, P. F. S. Rosa, C. Adriano, A. P. Reyes, P. L. Kuhns, P. G. Pagliuso, and R. R. Urbano, High field nuclear magnetic resonance in transition metal substituted $BaFe_2As_2$, J. Appl. Phys. **115**, 17D711 (2014).

[30] H. Wadati, I. Elfimov, and G. A. Sawatzky, Where Are the Extra *d* Electrons in Transition-Metal-Substituted Iron Pnictides? Phys. Rev. Lett. **105**, 157004 (2010).

[31] E. Granado, L. Mendonça-Ferreira, F. Garcia, G. de M. Azevedo, G. Fabbris, E. M. Bittar, C. Adriano, T. M. Garitezi, P. F. S. Rosa, L. F. Bufaiçal *et al.*, Pressure and chemical substitution effects in the local atomic structure of $BaFe_2As_2$, Phys. Rev. B **83**, 184508 (2011).

[32] P. F. S. Rosa, C. Adriano, W. Iwamoto, T. M. Garitezi, T. Grant, Z. Fisk, and P. G. Pagliuso, Pressure and chemical substitution effects in the local atomic structure of $BaFe_2As_2$, Phys. Rev. B **86**, 165131 (2012).

[33] P. F. S. Rosa, C. Adriano, T. M. Garitezi, M. M. Piva, K. Mydeen, T. Grant, Z. Fisk, M. Nicklas, R. R. Urbano, R. M. Fernandes, and P. G. Pagliuso, Possible unconventional superconductivity in substituted $BaFe_2As_2$ revealed by magnetic pair-breaking studies, Sci. Rep. **4**, 6252 (2014).

[34] P. F. S. Rosa, C. Adriano, T. M. Garitezi, R. A. Ribeiro, Z. Fisk, and P. G. Pagliuso, Electron spin resonance of the intermetallic antiferromagnet $EuIn_2As_2$, Phys. Rev. B **86**, 094408 (2012).

[35] M. G. Kim, R. M. Fernandes, A. Kreyssig, J. W. Kim, A. Thaler, S. L. Bud'ko, P. C. Canfield, R. J. McQueeney, J. Schmalian, and A. I. Goldman, Character of the structural and magnetic phase transitions in the parent and electron-doped $BaFe_2As_2$ compounds, Phys. Rev. B **83**, 134522 (2011).

[36] J. Zhao, W. Ratcliff II, J. W. Lynn, G. F. Chen, J. L. Luo, N. L. Wang, J. Hu, and P. Dai, Spin and lattice structures of single-crystalline, $SrFe_2As_2$, Phys. Rev. B **78**, 140504(R) (2008).

[37] K. Kaneko, A. Hoser, N. Caroca-Canales, A. Jesche, C. Krellner, O. Stockert, and C. Geibel, Columnar magnetic structure coupled with orthorhombic distortion in the antiferromagnetic iron arsenide, $SrFe_2As_2$, Phys. Rev. B **78**, 212502 (2008).

[38] A. Jesche, N. Caroca-Canales, H. Rosner, H. Borrmann, A. Ormeci, D. Kasinathan, H. H. Klauss, H. Luetkens, R. Khasanov, A. Amato *et al.*, Strong coupling between magnetic and structural order parameters in $SrFe_2As_2$, Phys. Rev. B **78**, 180504(R) (2008).

[39] D. W. Tam, W. Wang, L. Zhang, Y. Song, R. Zhang, S. V. Carr, H. C. Walker, T. G. Perring, D. T. Adroja, and P. Dai, Weaker nematic phase connected to the first order antiferromagnetic phase transition in $SrFe_2As_2$ compared to $BaFe_2As_2$, Phys. Rev. B **99**, 134519 (2019), and references therein.

[40] C. P. Poole and H. A. Farach, *Relaxation in Magnetic Resonance* (Academic Press, New York, 1971).

[41] S. Barnes, Theory of electron spin resonance of magnetic ions in metals, Adv. Phys. **30**, 801 (1981).

[42] A. Abragam and B. Bleaney, *Electron Paramagnetic Resonance of Transition Ions* (Oxford University Press, Oxford, UK, 2012).

[43] T. M. Garitezi, C. Adriano, P. F. S. Rosa, E. M. Bittar, L. Bufaiçal, R. L. de Almeida, E. Granado, T. Grant, Z. Fisk, M. A. Avila *et al.*, Synthesis and characterization of $BaFe_2As_2$ single crystals grown by In-flux technique, Braz. J. Phys. **43**, 223 (2013).

[44] A. Szytuła, Complex magnetic phenomena in f-electron intermetallic compounds, Material Science Poland **24**, 737 (2006).

[45] A. R. Denton and N. W. Ashcroft, Vegard's law, Phys. Rev. A **43**, 3161 (1991).

[46] R. R. Urbano, E. L. Green, W. G. Moulton, A. P. Reyes, P. L. Kuhns, E. M. Bittar, C. Adriano, T. M. Garitezi, L. Bufaiçal, and P. G. Pagliuso, Distinct High-$T$ Transitions in Underdoped $Ba_{1-x}K_xFe_2As_2$, Phys. Rev. Lett. **105**, 107001 (2010).

[47] F. J. Dyson, Electron spin resonance absorption in metals. II. Theory of electron diffusion and the skin effect, Phys. Rev. **98**, 349 (1955).

[48] G. Feher and A. F. Kip, Electron spin resonance absorption in metals. I. Experimental, Phys. Rev. **98**, 337 (1955).

[49] E. Dengler, J. Deisenhofer, H.-A. Krug von Nidda, S. Khim, J. S. Kim, K. H. Kim, F. Casper, C. Felser, and A. Loidl, Strong reduction of the Korringa relaxation in the spin-density wave regime of $EuFe_2As_2$, observed by electron spin resonance, Phys. Rev. B **81**, 024406 (2010).

[50] J. J. Ying, T. Wu, Q. J. Zheng, Y. He, G. Wu, Q. J. Li, Y. J. Yan, Y. L. Xie, R. H. Liu, X. F. Wang *et al.*, Electron spin resonance in $EuFe_{2-x}Co_xAs_2$ single crystals, Phys. Rev. B **81**, 052503 (2010).

[51] C. Rettori, H. M. Kim, E. P. Chock, and D. Davidov, Dynamic behavior of paramagnetic ions and conduction electrons in intermetallic compounds: $Gd_{1-x}Lu_xAl_2$, Phys. Rev. B **10**, 1826 (1974).

[52] X. Lu, D. D. Scherer, D. W. Tam, W. Zhang, R. Zhang, H. Luo, L. W. Harriger, H. C. Walker, D. T. Adroja, B. M. Andersen *et al.*, Spin Waves in Detwinned $BaFe_2As_2$, Phys. Rev. Lett. **121**, 067002 (2018).

[53] C. Liu, X. Lu, P. Dai, R. Yu, and Q. Si, Anisotropic magnetic excitations of a frustrated bilinear-biquadratic spin model: Implications for spin waves of detwinned iron pnictides, Phys. Rev. B **101**, 024510 (2020).

[54] T. Moriya, The effect of electron-electron interaction on the nuclear spin relaxation in metals, J. Phys. Soc. Jpn. **18**, 516 (1963).

[55] A. Narath, Nuclear magnetic resonance and relaxation of $^{197}$Au in gold metal and $^{109}$Ag in gold-silver alloys, Phys. Rev. **163**, 232 (1967).

[56] A. Narath and H. T. Weaver, Effects of electron-electron interactions on nuclear spin-lattice relaxation rates and Knight shifts in alkali and noble metals, Phys. Rev. **175**, 373 (1968).

[57] R. W. Shaw and W. W. Warren Jr., Enhancement of the Korringa constant in alkali metals by electron-electron interactions, Phys. Rev. B **3**, 1562 (1971).

[58] U. F. Kaneko, M. M. Piva, C. B. R. Jesus, M. E. Saleta, R. R. Urbano, P. G. Pagliuso, and E. Granado, Evidence of precursor orthorhombic domains well above the electronic nematic transition temperature in $Sr(Fe_{1-x}Co_x)_2As_2$, J. Phys.: Condens. Matter **31**, 495402 (2019).